Experimental and numerical study on cracking process in RC and R/FRC ties

Experimental and numerical study on cracking process in RC and R/FRC ties

Patrizia Bernardi

DICATeA – Department of Civil, Environmental, Land Management Engineering and Architecture, University of Parma, Italy

☎ +39 0521 90 5709

🗐 +39 0521 90 5924

patrizia.bernardi@unipr.it

www.unipr.it/dipartimenti/dicatea

Elena Michelini

DICATeA – Department of Civil, Environmental, Land Management Engineering and Architecture, University of Parma, Italy

☎ +39 0521 90 5709

🗐 +39 0521 90 5924

elena.michelini@unipr.it

www.unipr.it/dipartimenti/dicatea

Fausto Minelli

DICATAM – Department of Civil Engineering, Architecture, Land, Environment and Mathematics, University of Brescia, Italy

☎ +39 030 371 1223

🗐 +39 030 371 1312

fausto.minelli@ing.unibs.it

http://dicata.ing.unibs.it/minelli/

Giuseppe Tiberti

DICATAM – Department of Civil Engineering, Architecture, Land, Environment and Mathematics, University of Brescia, Italy

☎ +39 030 371 1221

🗐 +39 030 371 1312

giuseppe.tiberti@ing.unibs.it

ABSTRACT: A numerical non-linear procedure able to represent the behavior of cracked Steel Fiber Reinforced Concrete (SFRC) is herein presented and verified. The involved post-cracking mechanisms, particularly tension softening and tension stiffening, have been investigated and properly taken into account. Different tension softening relationships have been implemented and discussed, one based on a micro-mechanical approach, another obtained from inverse analysis and finally the Model Code 2010 (MC2010) law. These models have been adopted in conjunction with a smeared crack approach to perform FE simulations of R/FRC ties characterized by different

cross-sections and fiber volume fractions. Numerical results have been validated against a comprehensive experimental program on R/FRC (characterized by a tension softening behavior) and RC ties recently carried out at the University of Brescia. Comparisons between experimental and numerical results indicate that smeared models can be adopted also for the analysis of this structural typology, subjected to a uniaxial state of stress, as a valuable alternative to discrete approaches.

Keywords: Fiber reinforced concrete, Non-linear modeling, Tension stiffening, Tension softening, R/FRC ties.

1. Introduction

It is well established that the addition of fibrous reinforcement to concrete matrix enables to considerably increase the post-cracking residual tensile strength of the composite and, in general, its toughness. This enhanced capacity may allow for a reduction of conventional reinforcement (steel bars) especially in structures with high degree of redundancy, leading to an optimized reinforcement (i.e. higher performance at a lower cost) based on a combination of conventional steel bars and fiber reinforcement [1, 2]. This solution is particularly effective in terms of crack control – since a more distributed crack pattern characterized by reduced crack widths could be achieved – and also in terms of bearing capacity at Ultimate Limit States (ULS), since an adequate amount of rebars is still provided.

The increasing interest within the concrete community for Fiber Reinforced Concrete (FRC) is confirmed by its recent inclusion in the Model Code 2010 [3], which introduces as a key-parameter for structural applications the material performance. The latter is expressed in terms of four residual tensile strengths $f_{R,j}$, evaluated for different ranges of crack widths, each one relevant for different structural applications.

As mentioned, FRC significantly improves the behavior at Serviceability Limit States (SLS), with respect to crack and deflection control. In service conditions, steel-to-concrete bond allows the transfer of tensile stresses from the rebar to the surrounding concrete (between cracks), which stiffens the response of a Reinforced Concrete (RC) member subjected to tension. This stiffening effect, referred to as “tension stiffening”, has been studied by several authors in

traditional RC elements [4, 5] generally made of Normal Strength Concrete (NSC). It has been also verified that fibers exert a beneficial effect on this phenomenon, since their presence limits the growth of splitting cracks, similarly to the confinement action provided by ordinary stirrups. When the bond failure is instead governed by pullout, the influence provided by fibers on the local bond-slip response is more limited [6]. Furthermore, in FRC elements the post-cracking residual stresses due to fibers at any crack represent an additional contribution that influences the member response. The combination of these two mechanisms (tension stiffening and tension softening) results in a stiffer member behavior and in a different crack pattern, characterized by a reduced crack spacing and width.

With reference to experimental investigations, a number of research studies [7-9] were carried out so far on the tensile behavior of FRC members since late 90's. More recently, a broad experimental study on R/FRC members under uniaxial tension has been performed at the University of Brescia within a joint research with the University of Toronto [10, 11]. The main objective of this research was to evaluate formation and development of cracks in R/FRC members, both normal and high strength [12]. To this aim, a broad variety – not studied yet – of key-parameters have been considered, such as concrete compressive strength, element size, effective reinforcing ratio, rebar diameter, ϕ/ρ_{eff} ratio and volume fraction of fibers.

As regards theoretical analysis, several analytical approaches have been proposed for describing cracking phenomena in RC ties and, in general, in RC members (e.g.: [13-15]). More recently, Fantilli et al. [16, 17] have developed approaches, based on a proper discretization of the main solving differential equation, suitable for RC ties as well as for FRC ones.

Referring to finite element modeling, besides procedures based on the introduction of interface or connector elements between the steel bar and the surrounding concrete [18, 19], it is of main interest to take into account the peculiar combination of tension stiffening phenomenon between cracks with tension softening (provided by fibers at crack) in an unique smeared crack approach. One of the first studies was presented by Feenstra [20] for conventional reinforced concrete. Referring to concrete members reinforced by ordinary steel rebars and fibers, it can be mentioned the well known Disturbed Stress Field Model [21], which recently included the fiber resistant contribution [22]. Anyway,

these smeared approaches are more often applied to the analysis of beams, panels or slabs, while their application on R/FRC ties is rather limited [23, 24].

The present paper deals with the simulation of cracking phenomena in RC and R/FRC ties by means of non-linear numerical analyses based on a smeared-fixed crack approach [25, 26]. The numerical non-linear procedure has been suitably adapted for simulating the behavior of some FRC tension members with conventional reinforcement tested in the experimental campaign developed by Tiberti et al. [11]. Although in most structural applications FRC elements are co-reinforced with traditional reinforcement, studies on this topic are less common with respect to those focusing on members containing steel fibers only. More specifically, the proposed model allows the evaluation of the constitutive behavior of cracked FRC members by properly adding the contribution provided by fibers (in terms of tension softening and tension stiffening) to the resistant contributions due to concrete and traditional reinforcement bars. For the evaluation of tension softening, fiber bridging is directly added to the bridging effect provided by aggregates, whereas the influence exerted by fibers on tension stiffening is taken into account indirectly, by modifying the bond-slip law between ordinary steel bars and concrete (accordingly to [27]). The developed model enables a reliable prediction of the analyzed experimental results in terms of both bearing capacity and axial stiffness, also allowing an effective simulation of concrete cracking phenomena.

2. Experimental research

A comprehensive database of the behavior of R/FRC and RC ties containing a central steel rebar was generated in a broad experimental campaign developed at the University of Brescia [10, 11, 28].

A total number of 97 RC and R/FRC prismatic members were cast and tested. The following key-parameters were investigated:

- (square) cross-section side: from 50 to 200 mm;
- clear concrete cover: from 20 to 85 mm;
- effective reinforcing ratio, ρ_{eff} : from 0.98 to 3.26%;
- rebar diameter ϕ : 10, 20 and 30 mm;
- ϕ/ρ_{eff} ratio: from 306 to 2043 mm;

- specimen length: from 950 to 1500 mm;
- volume fraction of fibers V_f: 0, 0.5 and 1.0%.

The effective reinforcement ratio (ρ_{eff}) represents the rebar area over the area of concrete in tension surrounding the reinforcement: in the present samples, $\rho=\rho_{eff}$.

2.1 RC and R/FRC test specimen configurations

The experimental research was developed in two phases. In the first stage, 52 specimens having the geometry shown in Figure 1a were cast and tested. Each specimen was 950 mm long and five square cross-sections were selected: 50, 80, 100, 150 and 200 mm in size. In a second phase, only four square cross-sections were selected (80, 120, 180 and 200 mm in size) and a reinforcement ratio varying from 0.98% to 2.23% was adopted. Geometry and reinforcement details of specimens of the second phase are shown in Figure 1b.

All tests were performed under displacement control. Four Linear Variable Differential Transformers (LVDTs, one for each side), were employed to measure the mean deformation over the length of the specimen.

Samples belonging to the second stage of research, whose properties will be reported in next section, have been herein considered. More details concerning the overall experimental program can be found in Minelli et al. [10] and Tiberti et al. [11].

2.2 Material properties

All samples were cast with a normal strength concrete (NSC). The same basic mix design was used for all batches [10], i.e. cement content of 400 kg/m^3; water to cement ratio of 0.47; sand (0-4 mm) 610 kg/m^3; coarse aggregate (4-10 mm) 1132 kg/m^3; superplasticizer 3.3 l/m^3. With fibers, the amount of aggregate lowered up to a small 4%.

Low-carbon hooked-end macro fibers were used, characterized by a 30 mm length and 0.62 mm diameter (aspect ratio l/ϕ equal to 48), and with a tensile strength f_u=1270 MPa. Two volume fractions were adopted: 0.5 and 1% (0.5M and 1M in the following). Moreover, a reference batch without fibrous reinforcement was prepared (plain).

The concrete mechanical properties, as measured by means of standards tests (see [11]), are reported in Table 1 for the three batches. Even if the three concrete

mixes were designed to obtain the same nominal strength, the batch 1M was unfortunately characterized by a lower effective strength, making harder the comparison with the other specimens.

It should be also observed that all the specimens were stored in a fog room (R.H. > 95%; T=20 ± 2°C) until 2 or 3 days before testing; then they were air dried in the laboratory. In the fog room, the measured free shrinkage strains turned out to be negligible (around 20-25 micro-strains).

In order to characterize SFRC post-cracking behavior, three point bending tests (3PBTs) were also performed on small FRC notched beams (150x150x550 mm) according to EN 14651 [29]. Residual strengths $f_{R,j}$ (evaluated at 4 different Crack Mouth Opening Displacements - CMOD, i.e. 0.5, 1.5, 2.5 and 3.5 mm), and the flexural tensile strength (limit of proportionality) f_L were calculated, as reported in Table 2 (mean values).

Reinforcing bars (rebars) were made by B450C steel, according to European standard EN 10080 [30]. Tensile tests on rebars provided the mechanical properties reported in Table 3.

2.3 Main experimental results

The typical responses of RC and R/FRC ties, reported in Figure 2a, enables to emphasize one of the main advantages related to the combination of rebars and fibers, that is the global stiffness increase caused by the transmission of noticeable residual stress across cracks. This tendency can be recognized also during the crack formation stage but it is especially clear during the stabilized crack stage: in fact, as schematically shown in Figure 2a, the difference in tensile response at a given strain level, denoted by ΔLoad, illustrates the role of fibers. Hence, the tension stiffening increases with respect to that of RC samples.

Another significant investigated aspect concerns the crack pattern and its evolution in terms of mean crack spacing (s_{rm}). In Figure 2b, the evolution of the mean crack spacing s_{rm} is plotted as a function of the average strain up to the end of the crack formation stage for specimens N200/30 (N states for normal strength concrete, the first number represents the cross-section side in mm and the second one the bar diameter). From this plot, the reduction of the mean crack spacing, which represents the second main advantage due to the addition of fibers, can be clearly noticed.

Similar tendencies have been found in all other specimens; refer to Minelli et al. [10] and Tiberti et al. [11] for more details.

The experimental evidences will be numerically investigated in the following, by considering six R/FRC and RC ties, which, according to Tiberti et al. [11], are referred to as N120/20 and N180/20.

Table 4 summarizes the main different characteristics of the analyzed samples, in terms of geometrical dimensions and fiber contents.

3. Numerical modeling

The 6 considered ties have been analyzed through a numerical non-linear procedure, which is based on the implementation into a FE Code [31] of a suitable constitutive model for steel fiber reinforced concrete – named 2D-PARC – able to account both for the material non-linearity and for the resistant contribution offered by fibers.

The adopted constitutive model is based on a smeared-fixed crack approach and its theoretical formulation, which has been deduced for a SFRC membrane element subjected to general plane stresses, can be found in details in Cerioni et al. [25] and Bernardi et al.[26]. In short, the cracked SFRC stiffness matrix [*D*] is derived by considering the uncracked concrete and the steel reinforcement between adjacent cracks like two materials working in parallel, while uncracked SFRC between cracks and the crack itself are schematized like two elements working in series, so obtaining the following expression:

$$[D] = \left([D_c]^{-1} + [D_{cr1}]^{-1} \right)^{-1} \left([I] + [D_c]^{-1} [D_s] \right), \qquad (1)$$

where $[D_c]$ and $[D_s]$ are the stiffness matrices respectively of concrete and steel, $[I]$ is the identity matrix and $[D_{cr1}]$ represents the crack stiffness matrix. This latter accounts for the fundamental resistant mechanisms that take place after crack formation, that is aggregate and fiber bridging (in the following referred to as tension softening), aggregate interlock, tension stiffening and dowel action.

In next Sections the attention will be focused on the modeling of tension softening and tension stiffening, which represent the two main phenomena governing the behavior of cracked R/FRC ties, with particular reference to the influence exerted on them by steel fibers.

3.1 Tension softening

2D-PARC model is structured in a modular framework. All the mechanical phenomena governing the cracked stage are separately modeled on the basis of their properties. Subsequently these contributions are assembled to create an equivalent non-linear continuum material. In this way, each part of the model can be independently changed by adopting different formulations.

With regard to tension softening contribution, several semi-empirical relations have been implemented into the model (see [26]). In this work the micro-mechanical model proposed in [32] has been first followed. The transmission of tensile stresses across the crack due to aggregates and fibers is separately modeled; in more detail, aggregate bridging action is expressed through an empirical relation calibrated on the basis of several experimental data:

$$\sigma_{b1}(w_1) = \frac{\sigma_{ct\,max}}{1+(w_1/w_{01})^p} = c_{b1}\ \frac{w_1}{a_{m1}} = c_{b1}\ \varepsilon_1, \qquad (2)$$

where $\sigma_{ct\,max}$ is the maximum bridging stress due to aggregate action for a zero crack opening (so assumed equal to f_{ct}), w_1 is the crack width, w_{01} is the crack opening corresponding to 0.5 $\sigma_{ct\,max}$ and p is a parameter influencing the shape of the softening law. c_{b1} is the corresponding bridging coefficient to be inserted into the crack stiffness matrix [25] and ε_1 is the normal crack strain, which can be determined from the crack opening w_1 and the mean crack spacing a_{m1}. It should be observed that subscript *1* is generally referred to primary cracking according to the notation previously adopted in Cerioni et al. [25] and Bernardi et al. [26]. The model allows indeed the formation of multiple cracks (generically denoted by subscript *n*), characterized by a different orientation with respect to primary ones. These subsequent cracks have not been considered herein due to the uniaxial nature of the examined problem.

Fiber contribution σ_f is evaluated as the sum of fiber bridging σ_b and fiber prestress σ^0_{ps}, which characterizes fibers before the opening of a crack; both these terms can be expressed as a function of the total displacement s_1* across the crack itself, representing the resultant of crack opening w_1 and sliding v_1, according to Figure 3. The normal and tangential components of σ_f can be in turn evaluated through the following expressions:

$$\sigma_{f1}(s_1^*) = \sigma_f(s_1^*)\ \cos\omega_1 = \sigma_f(s_1^*)\ \frac{w_1}{\sqrt{w_1^2 + v_1^2}} = c_{f1}\ \varepsilon_1 \qquad (3)$$

$$\tau_{f12}(s_1^*) = \sigma_f(s_1^*)\ \sin\omega_1 = \sigma_f(s_1^*)\ \frac{v_1}{\sqrt{w_1^2 + v_1^2}} = c_{f1}\ \gamma_{12}\,, \qquad (4)$$

where c_{f1} represents the fiber coefficient, while $\varepsilon_1 = w_1/a_{m1}$ and $\gamma_{12} = v_1/a_{m1}$.

Both the terms related to aggregate bridging and fiber action are incorporated into the local crack stiffness matrix $[D_{cr1}]$ as part of the sub-matrix $[D_{c,cr1}]$, which takes into account the contribution of concrete at crack location. This latter can be expressed in the local coordinate system of the crack (n_1,t_1), as:

$$\left[\ D_{c,cr1}^{(n_1,t_1)}\ \right] = \begin{bmatrix} c_{b1} + c_{f1} & -c_{01} \\ 0 & c_{a1} + c_{f1} \end{bmatrix}, \qquad (5)$$

where c_{b1} and c_{f1} are the aforementioned coefficients (Eqs. 2-4), while c_{01} and c_{a1} schematize aggregate interlock effect [25].

As a second option, the evaluation of tension softening in R/FRC ties has been performed by implementing into 2D-PARC matrix the softening relation suggested in Model Code 2010 [3], which represents a useful tool in current design practice. It should be pointed out that the serviceability residual strength f_{Fts} and the ultimate residual strength f_{Ftu}, which are needed for the definition of the σ_n - w_1 curve, have been determined on the basis of the simplified post-cracking linear model proposed in MC2010 [3]. These variables are expressed as a function of the nominal residual strengths ($f_{R,j}$, Table 2) obtained by three point bending tests on SFRC notched beams. Since this σ_n - w_1 relation represents the post-cracking behavior of the composite material, by including both the contributions due to aggregates and fibers, the local crack stiffness matrix $\left[D_{c,cr1}^{(n_1,t_1)}\right]$ reported in Equation 5 must be in this case modified by considering a single coefficient c_{t1}, which has been derived as follows:

$$\sigma_n(w_1) = c_{t1}\frac{w_1}{a_{m1}} = c_{t1}\ \varepsilon_1\,, \qquad (6)$$

so replacing the corresponding (1,1) term $c_{b1}+c_{f1}$ in Equation 5.

Finally, a bilinear softening law formulated in terms of stress σ_n vs. crack opening w_1 has been obtained by means of the inverse analysis method [33]. To perform

inverse modeling, a bilinear softening diagram has been first assumed and numerical analyses of 3PBT on notched beams have been carried out. Subsequently, a best fitting procedure has been undertaken and the constitutive model optimized by minimizing the scatter between experimental and numerical analyses. Note that the elastic modulus (E_c) as well as concrete mean tensile strength (f_{ctm}) have been kept constant as they were experimentally determined (Table 1). For computational ease, these numerical analyses have been carried out by means of a discrete crack approach. The SFRC bilinear post-cracking law has been similarly implemented into the local crack stiffness matrix, by still considering a unique coefficient c_{t1} relative to the bridging effect of the composite material (concrete + fibers).

It should be underlined that all the three models described above are consistent with the performance approach (according to MC2010 [3]), in which the post-cracking behavior is a function of the composite material properties, not only of the adopted fibers. This also allows correctly modeling the fact that same fibers in different concretes would provide a rather different post-peak performance in the FRC composite.

According to the first softening law [32] this effect is taken into account by simply varying the bridging coefficient c_{b1}, while keeping constant the fiber coefficient c_{f1}. On the contrary, following the other approaches (MC2010 [3] and bilinear softening law) the single coefficient c_{t1} assumes different values according to the results of experimental material tests.

3.2 Tension stiffening

Tension stiffening effect has been included into 2D-PARC model by implementing – for each cracked integration point of the FE mesh – a proper bond-slip law into a numerical procedure based on the finite difference method. The non-uniform distribution of steel strains due to bond between steel and concrete amid adjacent cracks is indeed evaluated in a finite number of points along rebar axis (see [25]), by properly discretizing the solving differential equation:

$$\frac{d^2 s}{dx_i^2} = \frac{4}{\phi\ E_s} \left(1 + \frac{E_s}{E_c}\rho\right)\ \tau\ \left(s\ \left(x_i\right)\right), \qquad (7)$$

s being the slip between concrete and steel, τ the corresponding bond stress, ρ the geometrical steel percentage, ϕ the bar diameter and E_c, E_s the elastic moduli of concrete and steel. Thus, it is possible to evaluate the difference between the average and local stresses (at crack location) of the reinforcing bar, so as to properly model the increased stiffness of the bar in a cracked section due to bond [13]. The tension stiffening coefficient can be then evaluated as a function of the strain $\varepsilon_{si,cr1}$ of the i^{th} steel bar in correspondence of the crack:

$$g_{i1} = \frac{\varepsilon_{si,cr1}}{\delta_{i1}} \; l_{si}, \tag{8}$$

l_{si} being the length of the i^{th} bar between adjacent cracks and δ_{i1} the axial component, with respect to bar axis, of the crack displacement vector [25].

This resistant mechanism has been then incorporated into the local crack stiffness matrix $[D_{cr1}]$ as part of the sub-matrix $[D_{s,cr1}]$, which takes into account the contribution of steel reinforcement, so smearing the effect provided by bond. The matrix $[D_{s,cr1}]$ can be expressed in the local coordinate system of each reinforcement layer (x_i,y_i), as:

$$\left[\; D_{si,cr1}^{(x_i,y_i)} \; \right] = \rho_{si} \begin{bmatrix} \bar{E}_{si}^{cr1} \, g_{i1} & 0 \\ 0 & d_{i1} \end{bmatrix}, \tag{9}$$

$\bar{E}_{si}^{cr1}$ being the secant elastic modulus corresponding to the steel axial strain at the crack, g_{i1} the coefficient related to tension stiffening and d_{i1} the one representing dowel action, which is evaluated according to Walraven and Reinhardt [34]; see also Cerioni et al. [25]. As already known, the influence of dowel action can be neglected in the analysis of R/FRC ties; however its inclusion in 2D-PARC constitutive relation represents a potentiality of the model, which can be relevant in the study of other structural RC or FRC elements.

The sub-matrix specified in Equation 9 is first evaluated for each i^{th} reinforcement layer in its own local coordinate system (x_i,y_i), then transposed into the global system and summed up for all steel layers of the analyzed element.

With regard to the bond-slip law adopted for the resolution of Equation 7, the one proposed in Harajli [27] and Harajli and Mabsout [6] has been adopted, since it properly takes into account the effect exerted by steel fibers on global structural response. As reported in Figure 4a, fiber action is similar to that of transverse

reinforcement in reducing the development of splitting cracks and preventing the brittle failure that characterizes ordinary unconfined concrete. This effect can be then taken into account by explicitly introducing – in the governing equations – a sort of "confinement parameter", which depends on fiber volume percentage in the concrete matrix as well as on fiber geometry (namely diameter and length). In case of pull-out failure the influence of fibers is not significant and the local response in terms of bond stress-slip is similar to that of plain concrete; as a consequence, also the governing equations are quite similar – even if not identical – to those proposed in MC2010 [3] for ordinary reinforced concrete. Anyhow, the analytical formulation of this modified τ-s relation can be found in details in [26]. Since the law proposed in [6, 27] applies only for SFRC elements, the MC2010 τ-s relation [3], reported in Figure 4b, has been also implemented into 2D-PARC constitutive matrix, to allow the analysis of plain concrete samples, as discussed in the following.

The resulting bond-slip laws for the three considered experimental batches are shown in Figure 4c. Note that the three curves are almost superimposed for small values of slip, while, as slip increases, the batches with a progressively greater amount of fibers appear to be characterized by a less steep ascending branch and by a lower plateau corresponding to τ_{max} (and also to the residual bond strength τ_f). This effect is here not related to fibers but to the lower compressive strengths of the two FRC materials with respect to reference plain concrete (f_{cm} respectively equal to 47.2 MPa for plain concrete, 40.8 MPa for 0.5M and 27.4 MPa for 1M, according to Table 1). As an example, Figure 4d reports two typical bond-slip curves obtained by considering the same concrete strength, with or without fibers: for small values of slip the two curves are still almost identical, while, as slip increases, fibers determine a reduction in the slope of the ascending branch and an increase in the maximum value of bond strength τ_{max} and in the length of the corresponding plateau. It is worthwhile noticing that, in presence of pull-out failure, the law proposed in Harajli [27] and Harajli and Mabsout [6] is independent from the fiber content V_f, while this latter influences the trend of the curve in case of splitting failure (which has not been considered here, since the examined specimens did not show splitting cracks).

4. Verification of SFRC constitutive tensile laws

In order to properly verify the parameters of the adopted tensile constitutive laws included into 2D-PARC model for cracked SFRC, the previously described tests on small notched beams have been first simulated. The post-cracking behavior of these beams without ordinary reinforcement is indeed basically ruled by tension softening, and consequently their modeling allows verifying the effectiveness of the softening law.

To this scope, a mesh combining quadratic 8-node as well as triangular 6-node and 3-node 2D elements (the latter in the area around the notch to better capture stress localizations) has been defined. Figure 5a shows the adopted discretization, which has been performed only for one half of the notched beam, taking advantage of the symmetry.

Numerical analyses have been first carried out by considering the tension softening model usually implemented into 2D-PARC for FE simulations of SFRC material, namely the Li et al. [32] law. The trend of this softening law is mostly influenced by the choice of three main parameters – the snubbing coefficient *f*, the interfacial bond strength τ_0 and the orientation efficiency factor η_0 – for which a range of variability is suggested in [32], based on experimental data on SFRC specimens.

In this work, reasonable values, reported in Table 5, have been chosen for the three-abovementioned parameters (within the range suggested in [32]) on the basis of the properties of the considered batches. Although the type of fibers is the same, different values have been adopted for the two FRC batches, due to the lower strength of the 1M concrete matrix. Accordingly, these values of f, τ_0, η_0 (Table 5) have been also adopted for the FE simulations on R/FRC ties having the same concrete matrices and fiber contents. The good agreement between numerical and experimental behavior of notched beams in terms of applied load vs. CMOD response (Fig. 6a-b) confirms the adequacy of the adopted values.

The numerical modeling of notched beams has been subsequently performed by considering other two simplified tension softening relations: the MC2010 [3] law and the bilinear equation derived from inverse analysis.

A comparison between the three considered tensile laws is reported in Figure 5b (with reference to 0.5M matrix) in terms of both σ_n-w_1 and σ_n-ε_1, by assuming a structural characteristic length a_{m1} equal to the length of the adopted fibers (as can be found also elsewhere, like in [35]). The three responses are almost coincident

in the first part of the descending branch (for very small values of w_1), while, as crack opening increases, MC2010 [3] law tends to provide a greater fracture energy value for both small crack openings (less than 0.2 mm, typical of SLS, Serviceability Limit State) and for large crack widths. This trend is also confirmed by numerical analyses performed on notched beams through 2D-PARC model, by implementing the three abovementioned softening laws. As reported in Figure 6a-b (respectively referred to 0.5M and 1M specimens), a significant overestimation has been obtained by applying MC2010 [3] relation, while the simplified bilinear law and the one proposed by Li et al. [32] provide comparable responses, which also well fit the available experimental data, for both fiber contents.

5. Prediction of R/FRC ties post-cracking behavior

2D-PARC constitutive model has been then applied to the analysis of the 6 R/FRC and RC ties defined in Table 4. Also in this case, only one half of the tensile member has been considered, taking advantage of the symmetry of the problem, as shown in Figure 7 (with reference to specimens N180/20). This choice has been possible since cracks are assumed to be uniformly smeared. A FE mesh constituted by quadratic, isoparametric eight-node 2D elements with reduced integration (4 Gauss integration points) has been adopted and the same geometric steel ratio has been assigned to all elements, thus smearing also the influence of the steel bar over the whole cross-section. Numerical analyses have been performed under displacement control (in order to achieve a better numerical convergence), by applying an increasingly uniform displacement to all nodes belonging to the terminal section of the specimen.

5.1 Basic assumptions for NLFE analysis

In this Section some remarks on the basic assumptions adopted in the model – mainly concerning material strengths and crack spacing - are discussed, so as to allow a better comprehension of the graphs reported in the following.

FRC tensile behavior in the cracked stage has been modeled by considering the three different laws described in previous sections and shown in Figure 5b for the batch 0.5M ([32], MC2010 [3], bilinear law). Numerical analyses have been carried out by considering deterministic values of material tensile strength as well as of fracture parameters through the mesh (without directly taking into account

the unavoidable statistical variability affecting any experiment). However, an indirect method for considering the material variability was employed as follows. The state of stress in R/FRC ties is, in fact, basically uniform and the cracking process starts at the weakest spot, while the following cracks will occur on locations where the tensile strength of the concrete is always slightly higher. Therefore, the most reliable numerical description of this phenomenon could be adopting the characteristic concrete tensile strength for the first crack [15] and the mean tensile strength for the last. Accordingly, in the stabilized crack stage (where no new cracks occur, but existing widen) the mean mechanical concrete properties should be used.

Based on the aforementioned remarks, the three considered concrete tensile laws have been properly modified by adopting a characteristic value of concrete tensile strength and by assuming, as a first approximation, the post-cracking parameters in terms of mean material values. Consequently, it is expected that first crack load will be reasonable captured, whereas the R/FRC and RC ties behavior will be slightly underestimated especially at the beginning of stabilized crack stage (end of crack formation phase). During the stabilized crack stage, the residual post-cracking strength provided by fibrous reinforcement at crack locations plays a relevant role since it governs the amount of stresses that can be re-introduced by means of steel-to-concrete bond in the uncracked portions of concrete between cracks. Moreover, the concrete portions between cracks remains within the elastic range, which generally makes the adoption of concrete characteristic tensile strength not a limitation. This procedure is intended to be an appropriate approximation of the actual behavior of R/FRC and RC ties within the framework of a smeared approach since it indirectly and simply takes into account the main effects of statistical distribution of material mechanical properties.

In Figure 8a the constitutive laws obtained by considering the Li et al. [32] model ($v_1 = 0$) and by assuming as concrete tensile strength the mean value f_{ctm} or the lower bound $f_{ctk,0.05} = 0.7\, f_{ctm}$ (which is referred to 5% fractile), are reported. It should be noticed that this assumption is relevant only for very small crack openings (less than 0.1 mm). A negligible difference can be instead noticed as crack opening increases (for values bigger than 0.2-0.3 mm).

The same trend has been also confirmed by FE simulation of R/FRC ties as reported in Figure 8b, which shows a comparison between the numerical and

experimental response in terms of load vs. strain for R/FRC tie N180/20, with 0.5M fibers. It is confirmed that the major differences between the two responses can be observed for small strains – particularly around the first cracking load – while differences become negligible, as expected, in the stabilized cracking stage. However, it seems to be clear that the assumption of a lower value for f_{ct} allows achieving a best fitting of the experimental evidence, so confirming the assumption expressed by Bigaj [15]. For this reason, all the following numerical curves have been obtained by assuming a tensile strength equal to $0.7f_{ctm}$, although not explicitly declared in the corresponding Figures.

Numerical results have been also influenced by the assumptions concerning crack spacing. In the original formulation of 2D-PARC model [25], the cracked stage is assumed to be characterized by a fully developed crack pattern (corresponding to the stabilized crack stage), considering a constant value of a_{m1}. The spacing is evaluated through an "a priori" method based on the transmission length l_t, by adopting different expressions depending on the type of reinforcement (traditional bars and/or steel fibers), as well as on the number of reinforcing layers with different orientations (i.e. longitudinal bars and stirrups). In the examined case, crack spacing a_{m1} has been first set equal to $1.17\, l_{s,max}$ [11], being $l_{s,max}$ the introduction length proposed in MC2010 [3] for elements reinforced with both traditional bars and fibers. This last expression enables a rational evaluation of tensile stresses attained by steel fibers for a given crack width, and so it can be implemented in various analysis models and programs, being useful for predicting the structural behavior of R/FRC members. However, it should be noticed that the prediction of crack spacing in FRC composites is still a matter of discussion. Recent research works (e.g. [36]) have indeed proposed other relations that seem to allow a better modeling of experimental results in case of high strength fiber reinforced concrete elements.

The numerical response obtained by implementing the abovementioned MC2010 [3] expression is reported in Figure 9, in terms of applied load vs. average axial strain (Fig. 9a) and in terms of applied load vs. average crack width (Fig. 9b) for specimen N120/20, with 0.5M fibers. In the same Figure, the experimental response has been also compared to the numerical curve obtained by setting the crack spacing equal to the mean value recorded during the experimental tests in the stabilized cracked stage. The experimental values of average crack width have

been simply evaluated by the average elongation (measured by the 4 LVDTs) divided by the number of visible cracks. It should be remarked that numerical results shown in Figure 9 have been obtained by applying the softening law proposed by Li et al. [32]. It can be also noticed that the two numerical curves are almost superimposed and provide a good fitting of the experimental response, both in terms of global behavior and in terms of crack opening w_1.

Consequently, in the case of R/FRC ties, the proposed smeared model is able to correctly predict the axial stiffness (both in the uncracked and cracked stage), the yielding of rebars (through the adopted tension stiffening model), the ultimate sustainable load, as well as the evolution of average crack widths with applied loads, which represent some of the most significant quantities to be used in structural design. On the contrary, since these elements are subjected to a uniform state of stress, the model cannot be predictive with regard to crack spacing. However smeared models, like the one herein described, are also able to provide information on crack pattern evolution (in terms of crack spacing and position along the longitudinal element axis) when applied to the analysis of structural elements that are in general subjected to stress gradients (such as beams or slabs; see [26], [37-39]).

The investigated problem concerning tension ties represents a sort of "limit case" in which both cracks and rebar are smeared and the applied state of stress is uniform. Nevertheless, as illustrated before, this approach can represent an interesting alternative with respect to finite element methods commonly adopted in the literature for this type of structural elements, which are generally based on discrete approaches or which model only the cracks as smeared, by considering instead the reinforcement as discrete [40]. One of the peculiarities of the adopted approach is indeed related to the ability of taking into account both tension softening and tension stiffening contributions into the formulation of the constitutive model, so reducing the computation effort related to the construction of the FE mesh, since no interface elements, nor double nodes in the cracked sections are required.

Moreover, the particular nature of the considered problem and the availability of measured values of crack spacing allow a deepen study of the effectiveness of softening models available in technical literature for FE applications, which is one of the main objective of this work. For these reasons, it has been chosen to adopt

the mean experimental value of crack spacing in the numerical analyses reported in the following.

5.2 Main numerical results

Some of the main comparison between experimental and numerical curves obtained by applying all the above described tension softening models (Li et al. [32], MC2010 [3], bilinear law), and adopting the experimental measured value of average crack spacing are reported Figure 10. In case of plain concrete specimens, numerical analyses have been performed by only using the law proposed by Li et al. [32]. For comparison, bare bar response has been also plotted on the graphs. The comparisons between numerical and experimental curves (Fig. 10) highlight that the Li et al. [32] tension softening model as well as the bilinear law appear to be adequate in representing the experimental behavior. On the contrary, the adoption of the MC2010 [3] law yields to an overestimation of the softening contribution especially in the post-yielding branch (for larger crack widths), as already highlighted in Figures 5b and 6. However, it should be remarked that this law has been developed for design purposes and the same *fib* Bulletin N° 65 [3] suggests the use of more advanced constitutive laws in refined FE analyses.

Similar results have been also obtained for specimens N180/20 (Figure 11), which are characterized by the same bar diameter but a bigger cross-section. The numerical analyses have been again performed by considering the same modeling choices already described for specimens N120/20. From Figure 11 it emerges that the proposed approach is able to represent the global behavior of the examined R/FRC ties, even if, for all the adopted tension softening models, better results have been achieved for a lower fiber content. For these specimens, having a low longitudinal steel ratio ($\rho = 0.98\%$), the role of fibrous reinforcement in the stabilized crack stage as well as in the post-yielding branch can be better appreciated. For both R/FRC ties (0.5M and 1M, Figure 11b and c, respectively), it can be recognized a similar quite good prediction of the numerical curves based on Li et al. model [32] and bilinear law, even if, especially for R/FRC 1M sample (Figure 11c), a worse estimation in the stabilized crack stage and upon yielding can be observed. This trend appears even more pronounced when using the MC2010 [3] law.

Subsequently, FE analyses have been repeated by updating the average crack spacing a_{m1}, on the basis of the experimental distance between cracks measured at different values of the applied load ("evolutive crack spacing"), in order to evaluate the possible improvement in numerical results with respect to the classical formulation with a constant average crack spacing. Generally speaking, including the evolution of crack spacing in the analyses should allow a better representation of R/FRC tie global behavior in the first stage of crack formation. On the other hand, the two approaches should provide almost coincident results in the stabilized crack stage.

The results obtained from the two approaches (constant or evolutive crack spacing) are reported in Figure 12 for specimens N180/20 (in which only the tension softening law by Li et al. [32] has been used). It has been found indeed that the numerical behavior of these specimens (which are characterized by a larger concrete cover and, thus, lower longitudinal steel ratio), is more affected by the crack spacing value assumed during the analysis, differently from specimens N120/20. Even if the curves obtained by assuming an evolutive crack spacing better fit the experimental responses for a given fiber content (plain or 0.5 M), the classical formulation based on the average crack spacing seems to be however adequate in predicting the most significant involved parameters (axial stiffness, yielding of rebar, ultimate load, crack width), requiring a lower computation effort. The same results have been also reported in Figure 13a in terms of tension stiffening contribution, defined as the difference between the load carried by the R/FRC tie and the corresponding resisted by the bare bar (ΔLoad, Figure 2a) for a given strain, according to Fields and Bishoff [9] and Wu and Gilbert [41]. The same graph of Figure 13a better highlights the contribution due to fibers (with respect to the reference plain concrete specimen) in the post-cracking stage, from both an experimental and numerical point of view. For the same specimen typology, the higher toughness due to fibers significantly increases the tensile strength of concrete between adjacent cracks for a given value of the average axial strain, so determining in turn an increase of tension stiffening contribution. This behavior appears to be more significant when comparing plain concrete to 0.5M specimen, while the beneficial effects related to a further increase in fiber content are partially counteracted by the lower properties of concrete in 1M sample (which has not been plotted so as to improve the readability of the graph).

Finally, Figure 13b shows a comparison between experimental and numerical responses for the same N180/20 specimen with 0.5M fibers in terms of tension stiffening contribution, by reporting all the three tension softening models implemented into 2D-PARC matrix, while keeping constant a_{m1}. Similarly to previous graphs, the bilinear law and the Li et al. law [32] allow to achieve a better fitting of experimental results both in the stabilized cracking stage and in the post-yielding range.

6. Conclusions

In this paper refined non-linear FE analyses have been performed on normal strength R/FRC and RC ties, characterized by different geometries and fiber contents. 2D-PARC constitutive matrix for SFRC elements [26] has been applied to correctly model the improvement offered by the inclusion of fibers in concrete mixes on global structural behavior, especially under service loads. Suitable semi-empirical laws have been implemented to this aim. The tensile behavior of R/FRC elements has been analyzed by separately evaluating tension softening and tension stiffening, even though these two mechanisms are often modeled together and simply referred to as "tension stiffening" elsewhere. Tension stiffening has been herein simply related to bond between steel and concrete, taking into account the influence exerted by fibers indirectly, by adapting the shape of the bond-slip law.
The main conclusions of this work can be summarized as follows:
- even if discrete models are still more frequently adopted for the analysis of R/FRC ties, the smeared model herein proposed is able to correctly represent the behavior of these structural elements, provided that reliable tension softening and tension stiffening relations are included;
- the resistant contribution of fibers at crack (tension softening) has been modeled by considering three softening laws characterized by a different level of accuracy (Li et al. [32]; MC2010 [3]; bilinear law). The law proposed by Li et al. and the simplified bilinear relation based on inverse analysis provide a quite precise response. On the contrary, MC2010 [3] law tends to significantly overestimate the softening contribution offered by fibers, especially in the post-yielding branch (i.e. for higher values of crack opening). This tendency occurs also in the stabilized crack stage for specimens having low longitudinal steel ratios;

- a further improvement of numerical analyses has been obtained by considering a variable (evolutive) crack spacing instead of a constant value, the latter related to the stabilized crack stage. In fact, a better representation of the actual response of tensile members can be obtained, especially for low cracking values. However, the classical formulation of the adopted model, based on the average crack spacing, seems to be adequate in predicting the most significant structural parameters involved (axial stiffness, yielding of rebar, ultimate load and crack width), by requiring at the same time a lower computation effort;
- the effectiveness of numerical analyses, when applied to real case studies, is also related to a suitable estimate of crack spacing, that can be made based e.g. on code formulae, such as the one reported in MC2010 [3].

Acknowledgements

The contribution of M.Sc. Eng. Alice Sirico in data processing and modeling is gratefully acknowledged.

References

[1] di Prisco M, Plizzari GA, Vandewalle L (2009). Fibre reinforced concrete: new design perspectives. Mater Struct 42(9): 1261-1281.

[2] Tiberti G, Minelli F, Plizzari G (2014[a]). Reinforcement optimization of fiber reinforced concrete linings for conventional tunnels. Compos Part B-Eng 58: 199-207. doi: 10.1016/j.compositesb.2013.10.012.

[3] *fib* Bulletin N° 65 (2012). Model Code 2010 - Final draft, Volume 1. Model Code, ISBN 978-2-88394-105-2.

[4] Beeby AW (1971). The prediction of Cracking in Reinforced Concrete Members. Ph.D. Thesis, University of London.

[5] Borosnyói A, Balázs GL (2005). Models for flexural cracking in concrete: the state of the art. Struct Concr 6 (2): 53-62.

[6] Harajli MH, Mabsout ME (2002). Evaluation of bond strength of steel reinforcing bars in plain and fiber-reinforced concrete. ACI Struct J 99(4): 509-517.

[7] Mitchell D, Abrishami HH (1997). Influence of steel fibres on tension stiffening. ACI Struct J 94(6): 769-773.

[8] Bischoff PH (2003). Tension stiffening and cracking of steel fibre reinforced concrete. J Mater Civil Eng-ASCE 15(2): 174-182.

[9] Fields K, Bischoff P.H. (2004). Tension stiffening and cracking of high strength reinforced concrete tension members. ACI Struct J 101(4): 447-456.

[10] Minelli F, Tiberti G, Plizzari GA (2011). Crack Control in RC Elements with Fiber Reinforcement. ACI Special Publication "Advances in FRC Durability and Field Applications" 280(6), Corina-Maria Aldea & Mahmut Ekenel (eds.).

[11] Tiberti G, Minelli F, Plizzari G, Vecchio FJ (2014[b]). Influence of concrete strength on crack development in SFRC members. Cement Concrete Comp 45: 176-185, doi: 10.1016/j.cemconcomp.2013.10.004.

[12] Deluce JR, Vecchio FJ (2013). Cracking behavior of Steel Fiber-Reinforced Concrete members containing conventional reinforcement. ACI Struct J 110 (3): 481-490.

[13] Giurani E (1981). On the effective axial stiffness of a bar in cracked concrete. Studi e Ricerche 3: 205-226, Graduate School for the Design of RC Structures, Politecnico di Milano, Milan, (Italy).

[14] Somayaji S, Shah SP (1981). Bond stress versus slip relationship and cracking response of tension members. ACI J proceedings 78(3): 217-225.

[15] Bigaj AJ (1999) Structural dependence of rotation capacity of plastic hinges in RC beams and slabs. Ph.D. Thesis, Delft University of Technology.

[16] Fantilli AP, Ferretti D, Iori I, Vallini P (1998). Flexural deformability of reinforced concrete beams. J Struct Eng-ASCE 124(9): 1041-1049.

[17] Fantilli AP, Mihashi H., Vallini P (2007). Crack profile in RC, R/FRCC and R/HPFRCC members in tension. Mater Struct 40(10): 1099-1114.

[18] Rots J (1988). Computational modeling of concrete fracture. Ph.D. Thesis, Delft University of Technology.

[19] Bernardi P, Cerioni R, Ferretti D, Michelini E (2014[a]). Role of multiaxial state of stress on cracking of RC ties. Eng Fract Mech 123: 21-33. doi: 10.1016/j.engfracmech. 2014.02.011.

[20] Feenstra PH (1993). Computational aspects of biaxial stress in plain and reinforced concrete. Ph.D. Thesis, Delft University of Technology.

[21] Vecchio FJ (2001). Disturbed stress field model for reinforced concrete: implementation. J Struct Eng 127 (1): 12-20.

[22] Lee S-C, Cho J-Y, Vecchio FJ (2011). Diverse embedment model for steel fiber-reinforced concrete in tension: Model development. ACI Mater J 108 (5): 516-525.

[23] Lee S-C, Cho J-Y, Vecchio FJ (2013). Tension-stiffening model for steel fiber-reinforced concrete containing conventional reinforcement. ACI Struct J 110 (4): 639-648.

[24] Bernardi P, Michelini E, Minelli F, Sirico A, Tiberti G (2014[b]). Non-linear analyses and cracking process of FRC tension ties. Proc. of Computational Modelling of Concrete Structures (EURO-C 2014): 883-892, Bićanić et al. (eds), CRC Press/Balkema, Leiden, The Netherlands.

[25] Cerioni R, Iori I, Michelini E, Bernardi P (2008). Multi-directional modeling of crack pattern in 2D R/C members. Eng Fract Mech 75: 615-628. doi: 10.1016/j.engfracmech. 2007.04.012.

[26] Bernardi P, Cerioni R, Michelini E (2013). Analysis of post-cracking stage in SFRC elements through a non-linear numerical approach. Eng Fract Mech 108: 238- 250. doi: 10.1016/j.engfracmech.2013.02.024

[27] Harajli MH (2007). Numerical bond analysis using experimentally derived local bond laws: a powerful method for evaluating the bond strength of steel bars. J Struct Eng-ASCE 133(5): 695-705.

[28] Tiberti G, Minelli F, Plizzari G (2015). Cracking behavior in reinforced concrete members with steel fibers: A comprehensive experimental study. Cem Concr Res 68: 24-34. doi: 10.1016/j.cemconres.2014.10.011

[29] EN 14651-5 (2005): Precast Concrete Products – Test method for metallic fibre concrete – Measuring the flexural tensile strength, Europ. Standard.

[30] EN 10080 (2005): Steel for the reinforcement of concrete - Weldable reinforcing steel - General, Europ. Standard.

[31] ABAQUS 6.10 (2010). Online Documentation. Dassault Systémes Simulia Corp.

[32] Li VC, Stang H, Krenchel H (1993). Micromechanics of crack bridging in fibre-reinforced concrete. Mater Struct 26: 486-494.

[33] Roelfstra PE, Wittmann, FH (1986). Numerical method to link strain softening with failure of concrete, in “Fracture Toughness and Fracture Energy”, Edited by FH Wittmann, Elsevier, London.

[34] Walraven JC, Reinhardt HW (1981). Theory and experiments on the mechanical behaviour of cracks in plain and reinforced concrete subjected to shear loading. HERON 26 (1a), Delft University of Technology.

[35] Chiaia B, Fantilli AP, Vallini P (2009). Evaluation of crack width in FRC structures and application to tunnel linings. Mater Struct 42: 339-351.

[36] Deluce JR, Lee SC, Vecchio FJ (2014). Crack model for Steel Fiber-Reinforced Concrete members containing conventional reinforcement. ACI Struct J 111 (1): 93-102.

[37] Belletti B, Bernardi P, Cerioni R, Iori I (2003). On the behaviour of R/C beams without shear renforcement. Proc. of Computational Modelling of Concrete Structures (EURO-C 2003): 645-654, Bićanić et al. (eds), CRC Press/Balkema, Leiden, The Netherlands.

[38] Belletti B, Bernardi P, Meda A (2004). Shear behaviour of prestressed beams reinforced with steel fibers. Proc. of the 6th RILEM International Symposium (BEFIB 2004): 925-934, di Prisco et al. (eds), RILEM Publication SARL

[39] Bernardi P, Cerioni R, Michelini E (2012). Numerical modelling of the behaviour of SFRC elements in presence of multiple cracks, CD & Proc. book of abstracts of the 8th RILEM International Symposium (BEFIB 2012): 219-220, Barros et al. (eds), RILEM Publication SARL;

[40] Malecki T, Marzec I, Bobiński J, Tejchman J (2007). Effect of a characteristic length on crack spacing in a reinforced concrete bar under tension. Mechanics Research Communications 34: 460-465.

[41] Wu HQ, Gilbert RI (2009). Modeling short-term tension stiffening in reinforced concrete prisms using a continuum-based finite element model. Engng Struct 31: 2380-2391.

List of Figures

Fig. 1 Geometry and reinforcement details of specimens: (a) 1st and (b) 2nd phase (all dimensions in mm).

Fig. 2 (a) Typical responses and (b) evolution of the mean crack spacing of RC and R/FRC N200/30 ties.

Fig. 3 SFRC membrane element in the cracked stage: kinematical parameters of the crack.

Fig. 4 Adopted bond-slip laws: (a) Harajli [27] and Harajli and Mabsout [6]; (b) MC2010 [3]. Comparison of the adopted bond-slip law for (c) the three considered mixes and (d) for specimens with same the concrete strength, with and without fibers.

Fig. 5 (a) FE mesh of small notched beams (dimensions in mm); (b) tension softening laws considered for FE analyses on notched beams.

Fig. 6 Comparisons between experimental and numerical responses in terms of load vs. CMOD for (a) 0.5M and (b) 1M notched beams by considering different tension softening laws.

Fig. 7 FE mesh adopted for N180/20 tension ties (dimensions in mm).

Fig. 8 Influence of the assumed concrete tensile strength value on (a) Li et al. [32] tension softening model, (b) global behavior of N180/20 R/FRC tension tie, in terms of load vs. strain response.

Fig. 9 Comparisons between numerical and experimental response for N120/20 tie with 0.5M fibers by considering the experimental or the MC2010 [3] average crack spacing am_1 in terms of (a) load vs. average axial strain and (b) load vs. average crack width.

Fig. 10 Comparisons between numerical and experimental response for N120/20 (a) plain concrete, (b) 0.5M and (c) 1M R/FRC ties in terms of load vs. strain response. For 0.5M and 1M specimens, a comparison between different tension softening laws is also provided.

Fig. 11 Comparisons between numerical and experimental response for N180/20 (a) plain concrete, (b) 0.5M and (c) 1M R/FRC ties in terms of load vs. strain response. For 0.5M and 1M specimens, a comparison between different tension softening laws is also provided.

Fig. 12 Comparison between numerical and experimental response for 0.5M N180/20 R/FRC tie in terms of load vs. strain response by assuming Li et al. [32] softening law and different crack spacing (constant or evolutive).

Fig. 13 Comparisons between numerical and experimental response for N180/20 ties in terms of tension stiffening contribution vs. strain response by assuming (a) Li et al. [32] softening law, a variable (evolutive) or constant crack spacing and a different amount of fibers (plain concrete and 0.5M) or (b) different tension softening laws and a constant crack spacing.

List of Tables

Table 1 Concrete mechanical properties

Table 2 Fracture parameters of SFRC according to EN 14651

Table 3 Geometrical and mechanical properties of reinforcing steel bars (2nd phase)

Table 4 Geometrical characteristics and fiber contents of investigated specimens

Table 5 Assumed values for parameters of Li et al. [32] law

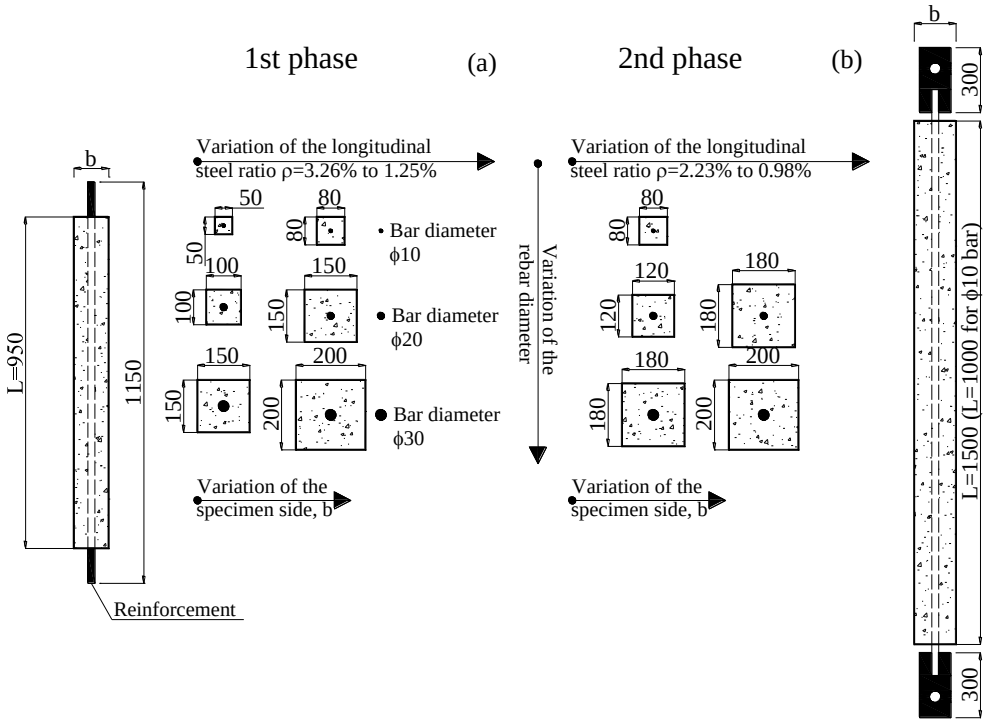

Fig. 1 Geometry and reinforcement details of specimens: (a) 1st and (b) 2nd phase (all dimensions in mm).

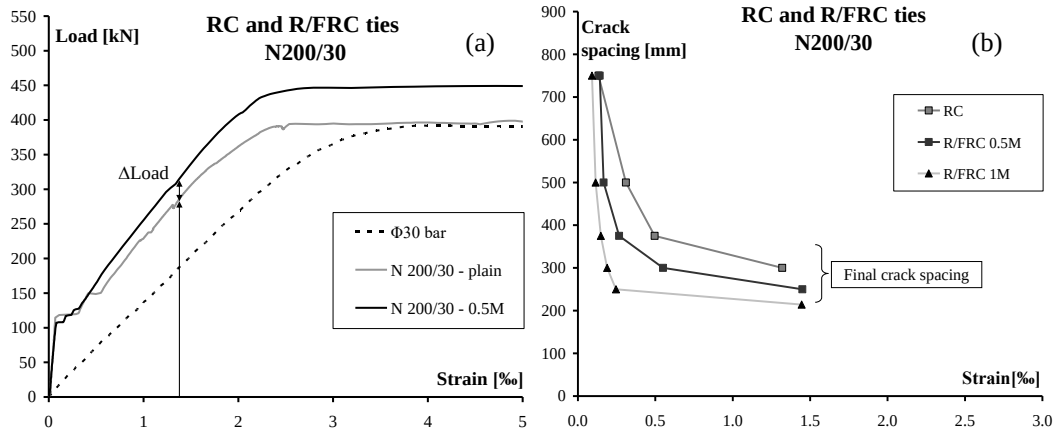

Fig. 2 (a) Typical responses and (b) evolution of the mean crack spacing of RC and R/FRC N200/30 ties.

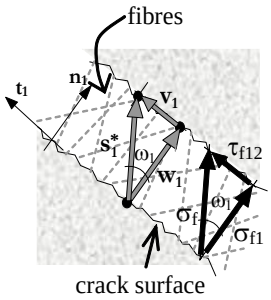

Fig. 3 SFRC membrane element in the cracked stage: kinematical parameters of the crack.

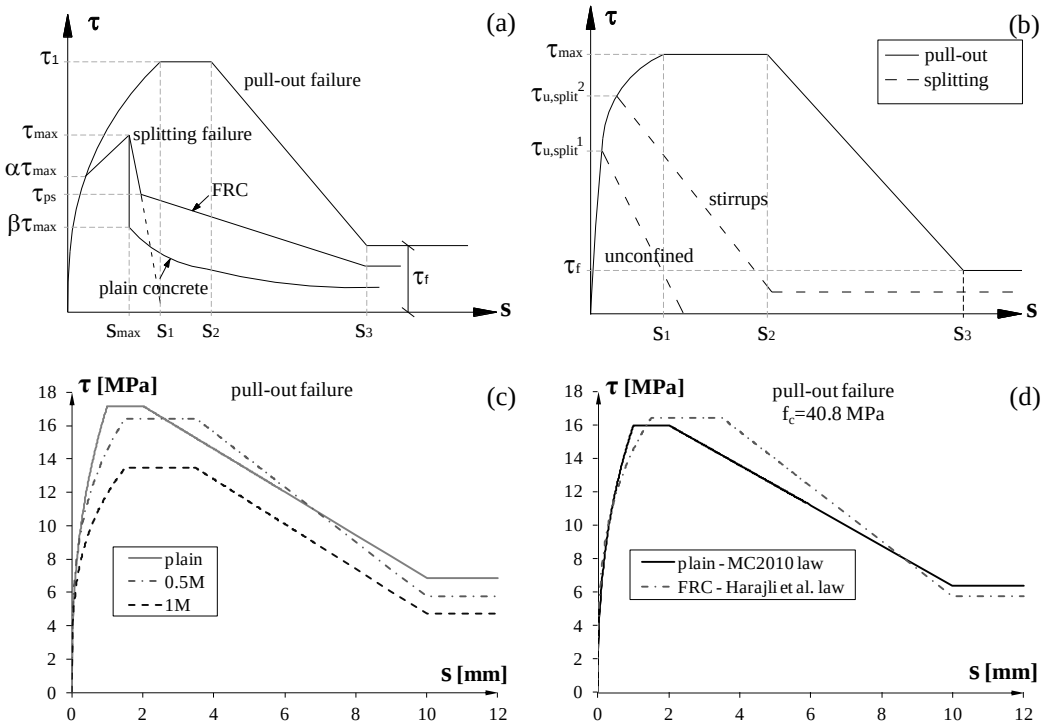

Fig. 4 Adopted bond-slip laws: (a) Harajli [27] and Harajli and Mabsout [6]; (b) MC2010 [3]. Comparison of the adopted bond-slip law for (c) the three considered mixes and (d) for specimens having the same concrete strength, with and without fibers.

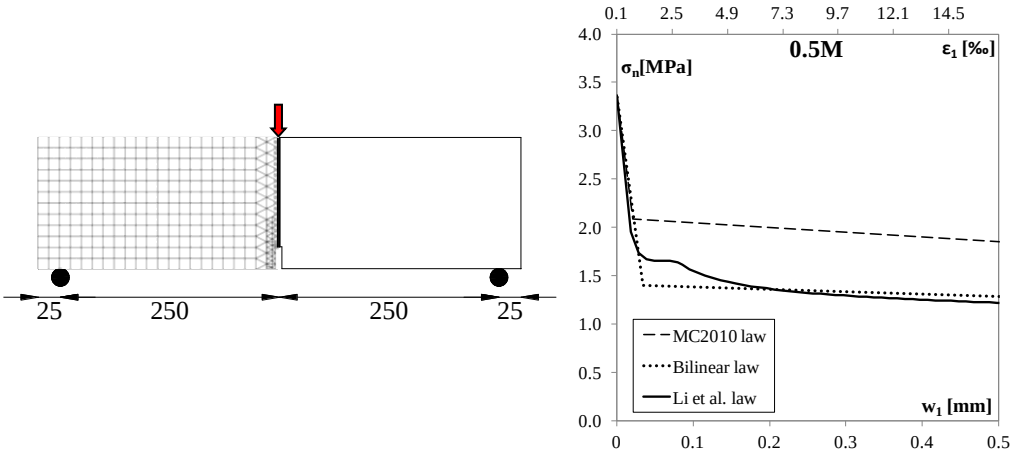

(a) (b)

Fig. 5 (a) FE mesh of small notched beams (dimensions in mm); (b) tension softening laws considered for FE analyses on notched beams.

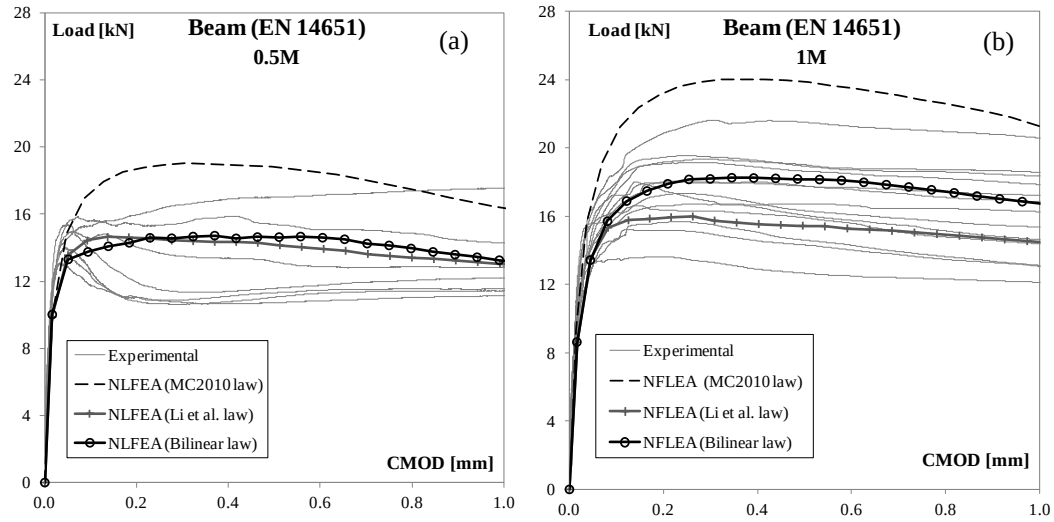

Fig. 6 Comparisons between experimental and numerical responses in terms of load vs. CMOD for (a) 0.5M and (b) 1M notched beams by considering different tension softening laws.

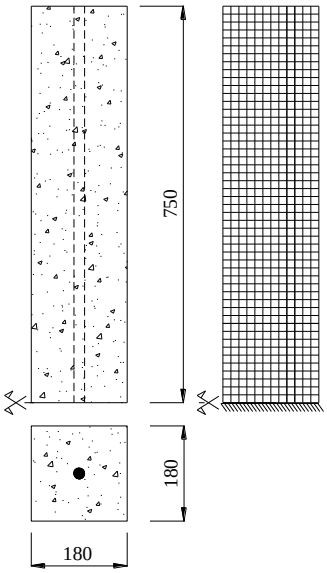

Fig. 7 FE mesh adopted for N180/20 R/FRC tension ties (dimensions in mm).

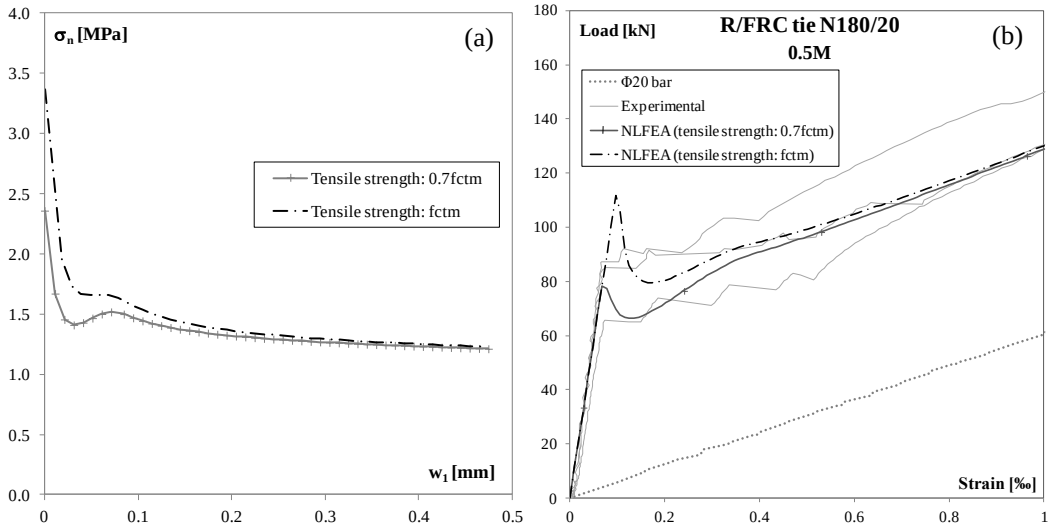

Fig. 8 Influence of the assumed concrete tensile strength value on (a) Li et al. [32] tension softening model, (b) global behavior of N180/20 R/FRC tie, in terms of load vs. strain response.

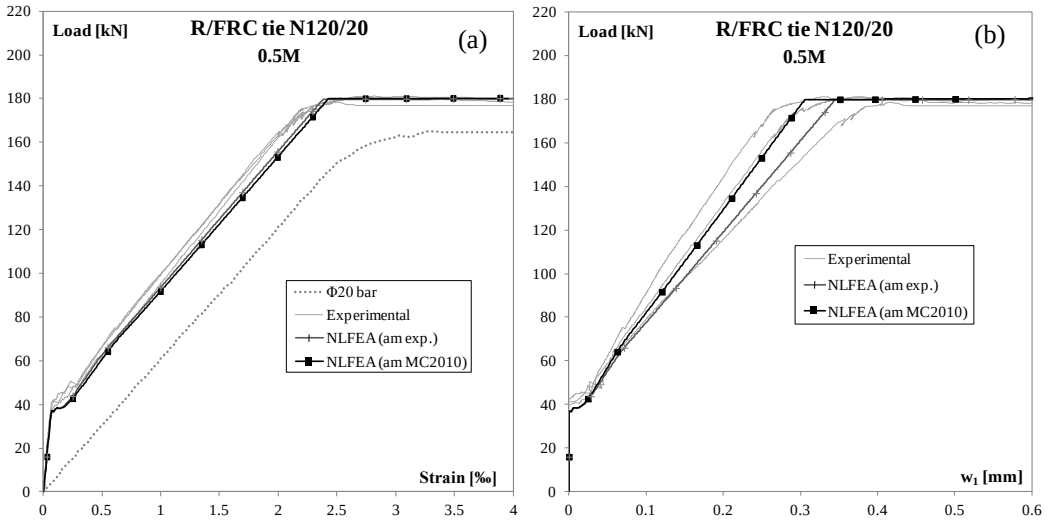

Fig. 9 Comparisons between numerical and experimental response for N120/20 tie with 0.5M fibers by considering the experimental or the MC2010 [3] average crack spacing am_1 in terms of (a) load vs. average axial strain and (b) load vs. average crack width.

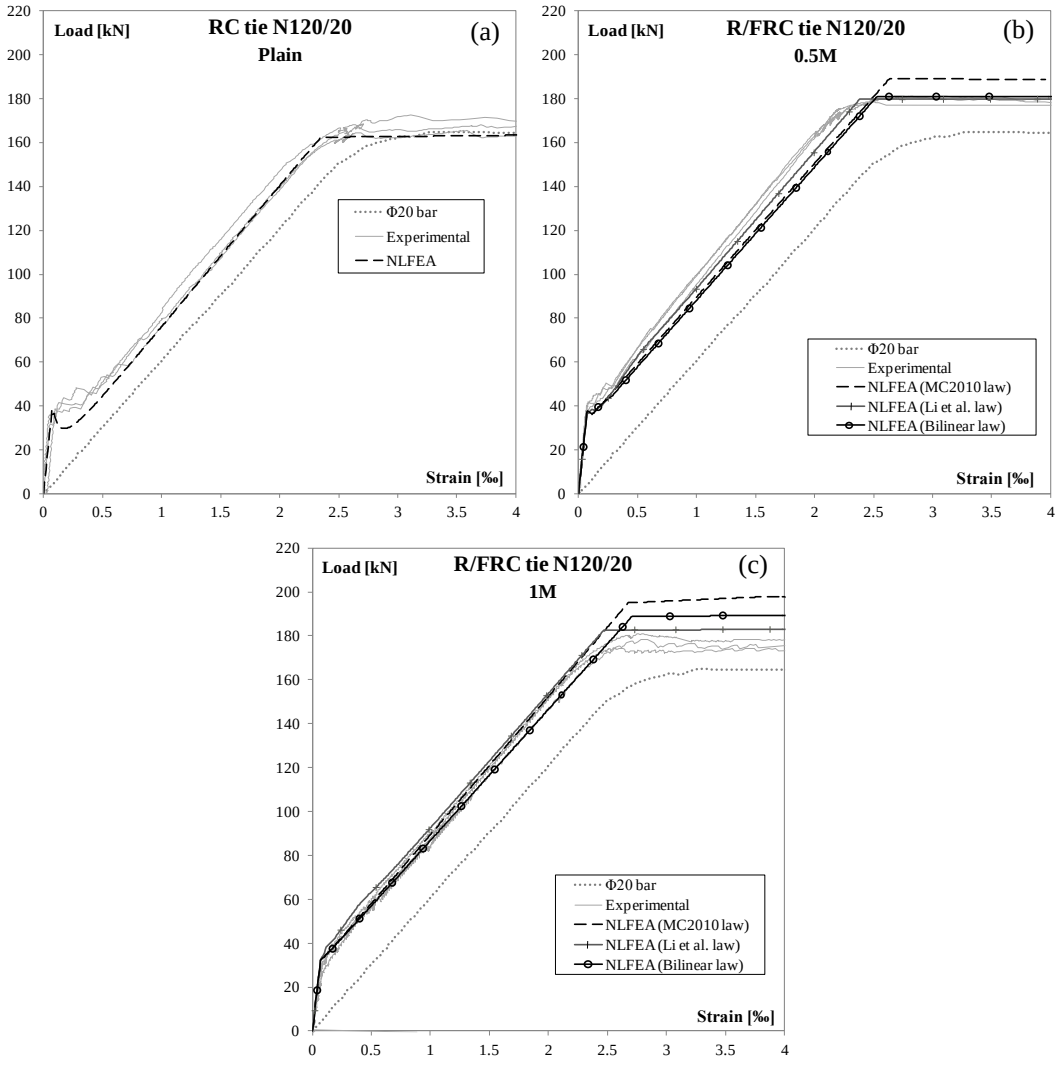

Fig. 10 Comparisons between numerical and experimental response for N120/20 (a) plain concrete, (b) 0.5M and (c) 1M R/FRC ties in terms of load vs. strain response. For 0.5M and 1M specimens, a comparison between different tension softening laws is also provided.

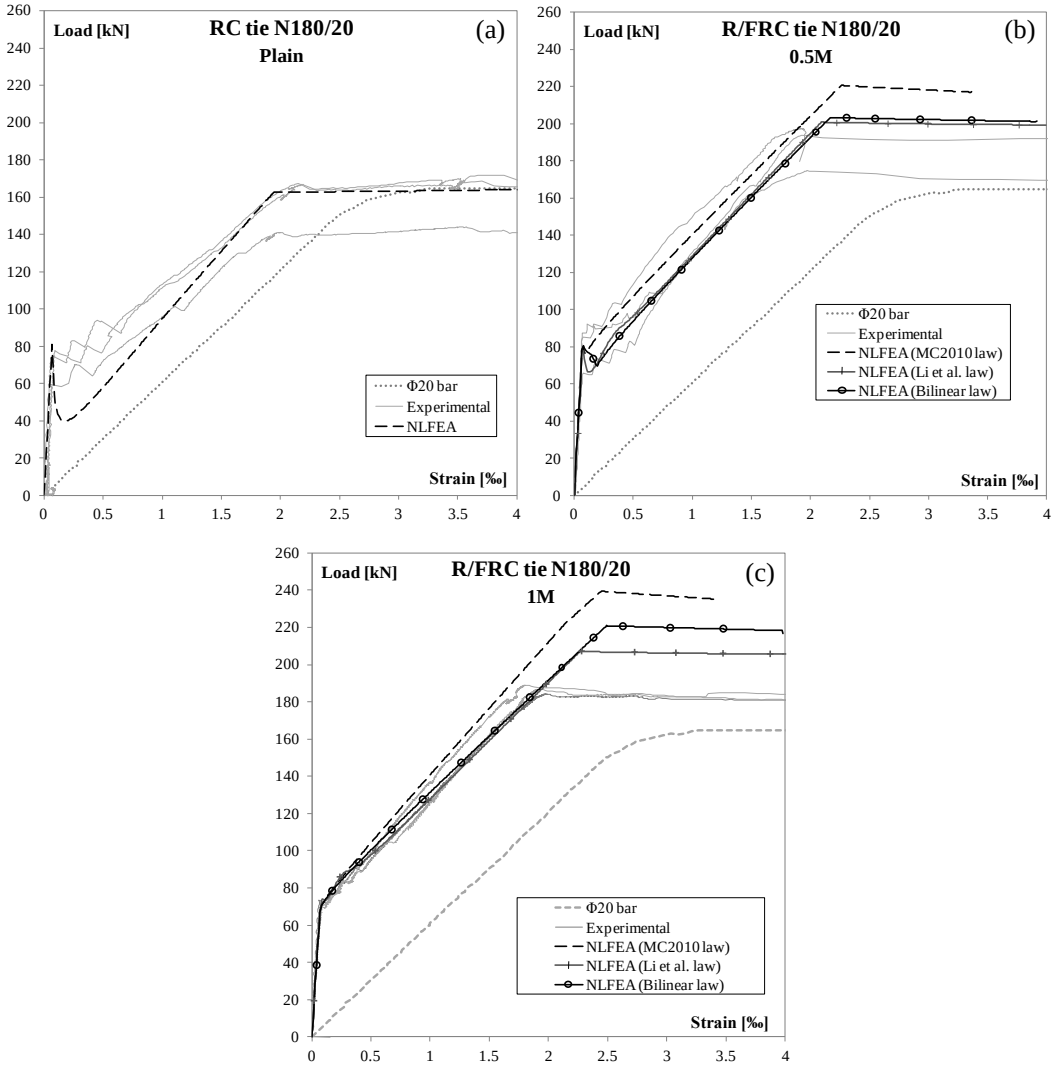

Fig. 11 Comparisons between numerical and experimental response for N180/20 (a) plain concrete, (b) 0.5M and (c) 1M R/FRC ties in terms of load vs. strain response. For 0.5M and 1M specimens, a comparison between different tension softening laws is also provided.

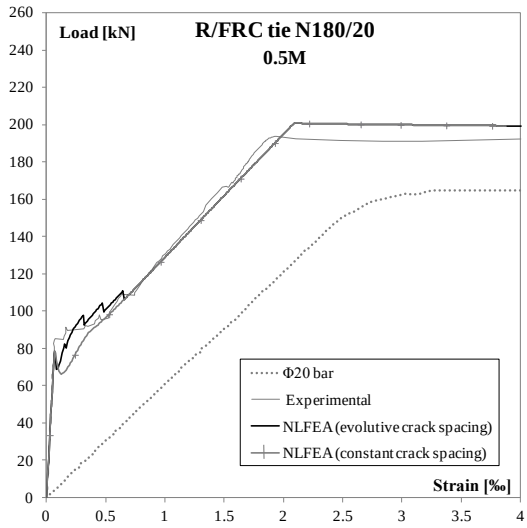

Fig. 12 Comparison between numerical and experimental response for 0.5M N180/20 R/FRC tie in terms of load vs. strain response by assuming Li et al. [32] softening law and different crack spacing (constant or evolutive).

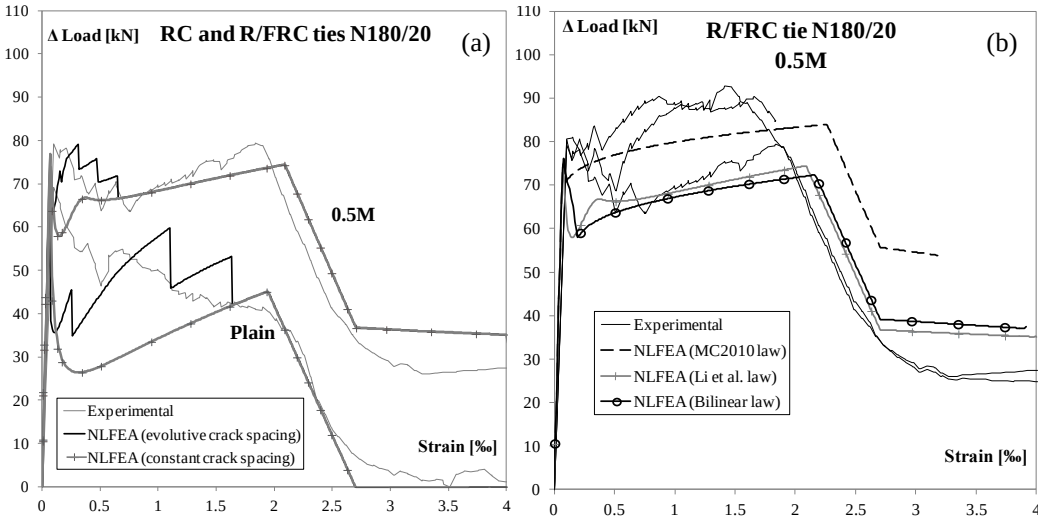

Fig. 13 Comparisons between numerical and experimental response for N180/20 ties in terms of tension stiffening contribution vs. strain response by assuming (a) Li et al. [32] softening law, a variable (evolutive) or constant crack spacing and a different amount of fibers (plain concrete and 0.5M) or (b) different tension softening laws and a constant crack spacing.

Table 1 Concrete mechanical properties

	plain	0.5M	1M
f_{cm} [MPa]	47.2	40.8	27.4
f_{ctm} [MPa]	3.50	3.35	2.85
E_c [MPa]	33900	32600	27800

Table 2 Fracture parameters of SFRC according to EN 14651

SFRC matrix	f_{Lm} [MPa]	f_{R1m} [MPa]	f_{R2m} [MPa]	f_{R3m} [MPa]	f_{R4m} [MPa]
0.5M	4.60	4.12	4.07	3.35	2.69
1M	4.64	5.43	4.89	4.36	3.86

Table 3 Geometrical and mechanical properties of reinforcing steel bars (2nd phase)

Diameter ϕ [mm]	A_s [mm^2]	E_s [GPa]	f_y [MPa]	f_t [MPa]
10	78	204	522	624
20	314	192	515	605
30-1†	707	192	554	672
30-2†	707	189	484	604
† - The ϕ30 bars came from two different production heats.				

Table 4 Geometrical characteristics and fiber contents of investigated specimens

Tension tie	N120/20 plain	N120/20 0.5M	N120/20 1M	N180/20 plain	N180/20 0.5M	N180/20 1M
Side [mm]	120			180		
Reinforcing bar [mm]	20			20		
Length [mm]	1500			1500		
Reinforcing bar ratio, ρ [%]	2.23%			0.98%		
V_f [%]	0	0.5	1	0	0.5	1

Table 5 Assumed values for parameters of Li et al. [32] law

Fibers	f	τ_0	η_0
0.5M	0.75	5.5	1.0
1M	0.50	4.0	1.0